ASPECT-DEPENDENT SCATTERING IN WIDEBEAM SYNTHETIC APERTURE SONAR

Stig Asle Vaksvik Synnes[a,b] , Roy Edgar Hansen[a,b]

[a] Norwegian Defence Research Establishment (FFI), PO Box 25, NO-2027 Kjeller, Norway.
[b] University of Oslo (UiO), Department of Informatics PO Box 1080, Blindern, N-0316 Oslo, Norway.

Contact author: Stig Asle Vaksvik Synnes,
Norwegian Defence Research Establishment (FFI), PO Box 25, NO-2027 Kjeller, Norway.
E-mail: Stig-Asle.Synnes@ffi.no

Abstract: *Widebeam synthetic aperture sonar (SAS) gathers information on the acoustic scattering over a scene. From the aspect-dependent scattering of facets we can extract information on their orientation and size. This is information that can be useful in target detection and classification.*

Each pixel of a SAS amplitude image represents the backscattering at a given location. In SAS imaging the backscattering is normally assumed to be independent of look angle within the beamwidth. This assumption of aspect-independent scattering is only valid for narrowbeam systems. For widebeam systems the backscattering of real scatterers can show a strong angular dependency over the beamwidth. We suggest to extract this additional information, and investigate the aspect-dependency of the backscattering going into each pixel. We are able to estimate both the orientation of facets and their size. We demonstrate the method on SAS data recorded from a HUGIN autonomous underwater vehicle using a HISAS system with a prototype low frequency transmitter covering the band 12-38 kHz with a -3dB beamwidth exceeding 100 degrees at the center frequency. The approach is based on adaptive matched filter feature extraction developed in synthetic aperture radar (SAR).

Keywords: *Synthetic aperture sonar, matched filter imaging, target response.*

1. INTRODUCTION

In synthetic aperture sonar (SAS) imaging algorithms, the backscattering is normally assumed to be independent of look angle. This assumption is usually not met when processing wide beamwidths. For example man-made objects with facets exhibit a strong aspect-dependent back-scattering, whereas other objects, such as small rocks, can reflect more like point-targets. This is the notion behind a series of feature-extraction and detection algorithms developed for synthetic aperture radar (SAR) [1, Section VII.C]. We recognize the methods presented in [2], [3] and [4] as the most fundamental of these. Rather than assuming isotropic backscattering during the imaging, they suggest to perform *adaptive matched filtering* in order to estimate size and orientation of the dominating scatterers (assumed planar) for each pixel, and they also build an *adaptive matched filter image*. The approach has been followed-up only to a small extent in SAR. Within SAS one related study extracts the dominating orientation and size, represented by coherence length of targets, though only on (simulated) target snippets and not individual pixel level data [5].

In this paper we focus on pixel level *feature extraction*. We suggest to use the features as *complementary information* to the original SAS image. One potential beneficial application is target recognition.

2. METHOD

The angular contribution to an image pixel is obtained by delaying the pulse compressed signal of each transmitter-receiver element along the aperture until they all focus onto the pixel. In traditional SAS imaging the contribution from each aperture element (all look angles) are then averaged to give the pixel intensity. In adaptive matched filter SAS imaging and feature extraction,we do matched filtering on this angular scattering information in place of summation.

We suggest an alternative approach for extracting the angular contribution of the scattering from a single look complex SAS image. The SAS image is transformed into the image wavenumber domain through a 2D Fourier transform, focused onto each pixel position, and the angular dependency of the scattering is extracted.

2.1 Example Image

We form the widebeam SAS image in accordance with the wideband back projection (WBP) approach of [6] [7]. For demonstrating the approach, we choose the low frequency (LF) SAS image of Fig. 1. The image data was recorded using FFI's HUGIN-HUS autonomous underwater vehicle (AUV) outside Horten in 2012 using the HISAS synthetic aperture sonar with a prototype LF transmitter. The LF band covers 12-38 kHz and was recorded concurrently with a medium frequency (MF) band covering 60-85 kHz. The scene contains targets of opportunity at 70 m depth and approximately 50 m ground range.

We assure maximum *angular coverage* by addressing images with samples evaluated at a spacing d_x equal to or smaller than that supported by our sensor and the image processing ($d_x = 2\pi/\Delta K_x \leq 2\pi/\Delta K_{x,max\_theo}$) [7]. We assure a good *angular resolution* by addressing images with hundreds of along-track samples, thus supporting the same number of image wavenumber bins.

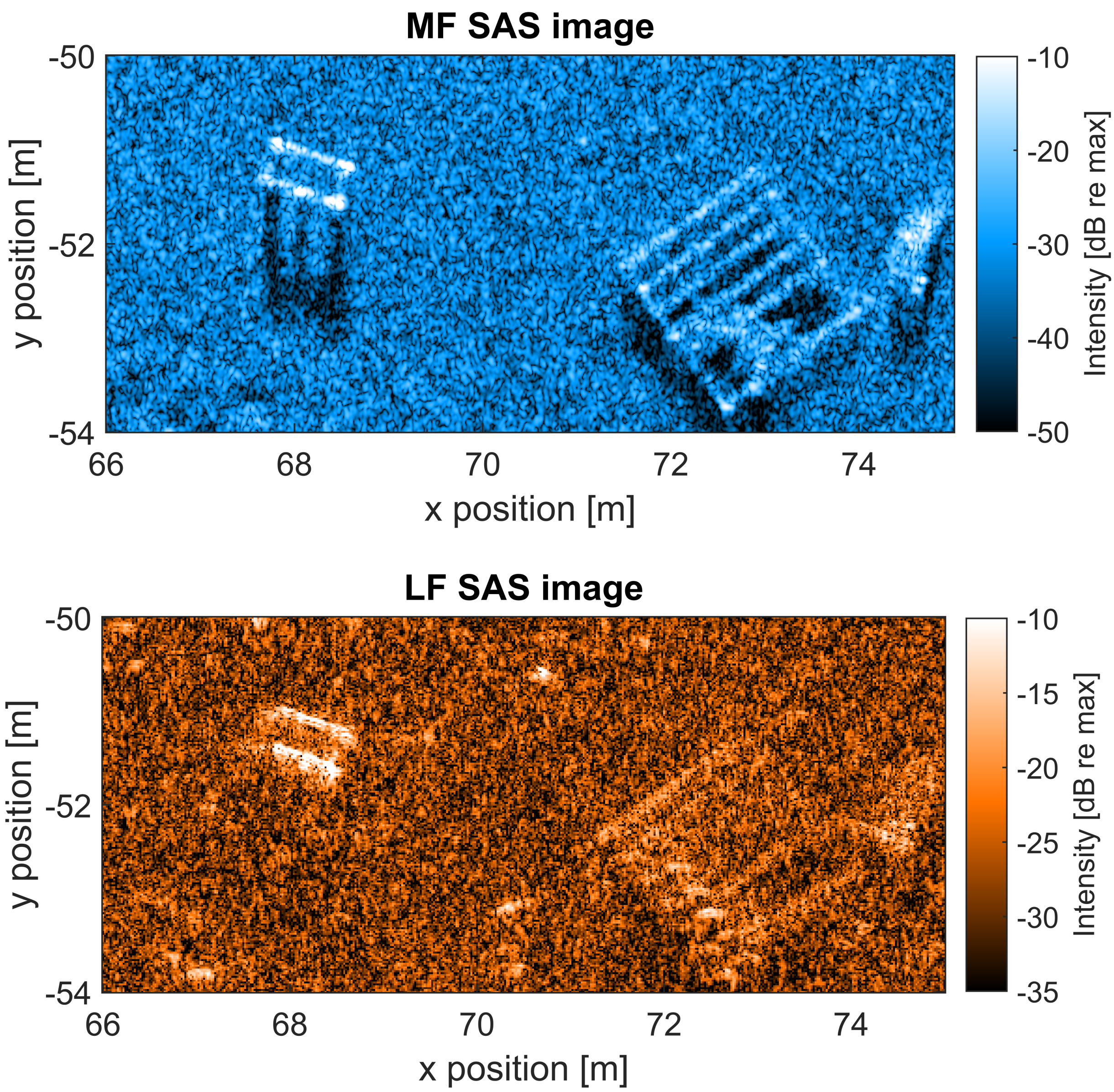

Fig. 1: SAS images of the example scene generated from concurrently recorded MF and LF data, using the HISAS 1030 on FFI's HUGIN HUS AUV with a LF prototype transmitter. The LF band spans 12-38 kHz with a center frequency beamwidth of 106 degrees, and the MF band spans 60-85 kHz with a center frequency beamwidth of 32 degrees.

2.2 Wavenumber Domain Focusing

We let h denote the SAS pixel value. Using the Matlab implementation of the Fourier transform, and ignoring the shift, we obtain:

$$H[\mu,\eta] = \sum_{m=1}^{M}\sum_{n=1}^{N} h[m,n]\cdot e^{-i2\pi(\mu-1)(m-1)/M}\cdot e^{-i2\pi(\eta-1)(n-1)/N}, \tag{1}$$

where $m \in [1, M]$ and $\mu \in [1, M]$ address the along-track pixel number and image wavenumber component and $n \in [1, N]$ and $\eta \in [1, N]$ the corresponding across-track indices. The individual pixel values can be reconstructed using the inverse Fourier transform:

$$h[m,n] = \sum_{\mu=1}^{M} \sum_{\eta=1}^{N} \frac{H[\mu,\eta]}{MN} \cdot e^{i2\pi(\mu-1)(m-1)/M} \cdot e^{i2\pi(\eta-1)(n-1)/N}. \tag{2}$$

The term inside the summations of (2) contains data from $H([\mu,\eta])$ focused onto image pixel $[m,n]$ and we denote these $F([\mu,\eta])|_{[m,n]}$.

In the above relations, the indices $[m,n]$ address the position $\vec{x} = (x[m], y[n])$, and the indices $[\mu,\eta]$ address the image wavenumber vector, $\vec{K} = (K_x[\mu], K_y[\eta])$. The Image wavenumber vector is related to the acoustic wavenumber vector $\vec{k}$ through the combined incident and reflected waves, $\vec{K} = \vec{k}_{re} - \vec{k}_{in}$. Thus we have $|\vec{K}| = 2|\vec{k}| \approx 4\pi/\lambda$, and $\angle\vec{K} = \arctan(K_x/K_y) = \theta$, where λ represents the wavelength and θ the look angle off broadside and defined positive counter-clockwise.

By collecting all the wavenumber domain components focused onto a single pixel before summation, we have decomposed the pixel contributions to individual frequencies and aspects. These data also contain information on all other pixels, but while these contributions are incoherent, the contribution for the pixel will be coherent over (nearby) aspects and frequencies. The approach can be summarized as follows:

$$\boxed{h(x,y) \rightarrow H(K_x,K_y) \rightarrow F(K_x,K_y)|_{(x_i,y_i)}}$$

Changing the focus point by similar approaches is also applied in fixed focusing for enhancement of shadows and elastic scattering [8] [9].

The image wavenumber domain intensity spectrum $|H(K_x,K_y)|$ of our example scene is shown in Fig. 2. By changing focusing point, the phase $\angle H(K_x,K_y)$ is altered while the intensity spectrum remains the same.

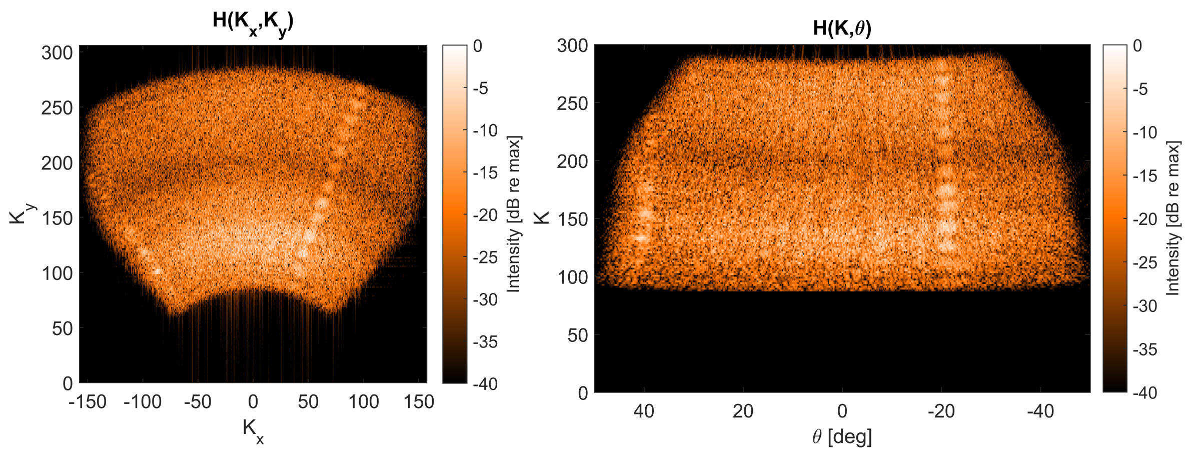

Fig. 2: Amplitude spectrum for the LF SAS image of Fig. 1, represented as function of image wavenumber in Cartesian coordinates (left) and polar coordinates (right). The effective beamwidth is limited to 90 degrees due to limited recording range.

2.3 Matched Filtering

At each pixel location, the focused wavenumber domain data can be matched to candidate target responses with potentially better match than that of an isotropic scatterer. In [2], [3] and [4], it is suggested to match-filter for linear (dihedral) targets of a few different lengths and many candidate orientations. We adopt their general approach, and extend it to cover the response of any linear scatterers (or rectangular facets), with length d and orientation (expressed by broadside direction) θ.

2.3.1 Uniform Linear Scatterer

The scattering response of a uniform linear scatterer resembles the beampattern of a uniform linear array. This is well known to be represented by a sinc-function. A linear scatterer with broadside at angle θ will give (a frequency-independent) maximum scattering for look angles of θ. In the image wavenumber domain, the scattering strength will change only with distance orthogonal to the line described by θ, and follow a sinc pattern. The -3 dB bandwidth ΔK_{-3dB} of the sinc-function follows from the length of the scatterer, D, as

$$\Delta K_{-3dB} \approx \Delta K_{00/2} = 2\pi/D, \tag{3}$$

where $\Delta K_{00/2}$ is half the zero-crossing bandwidth. This image wavenumber domain metric can be transformed to the beamwidth β at any frequency-dependent wavelength through

$$\beta = 2\arcsin(\lambda/2D). \tag{4}$$

In this study we ignore the full sinc beampattern and match to the scattering response described through its mainlobe only.

2.3.2 Orientation Estimation

The orientation of an uniform linear scatterer at position (x_i, y_i) can be found by locating the look angle with the maximum coherent signal. We address the image wavenumber domain spectrum $F(K_x, K_y)|_{(x_i,y_i)}$ and apply a Cartesian to polar transform (left to right panel in Fig. 2). Next we average over the K-axis to obtain the orientation dependency of the scattering $f(\theta)|_{(x_i,y_i)}$. The approach can be summarized as follows:

$$\boxed{F(K_x, K_y)|_{(x_i,y_i)} \rightarrow F(K, \theta)|_{(x_i,y_i)} \rightarrow f(\theta)|_{(x_i,y_i)}}$$

Next we examine the orientation dependency of the scattering in order to find the orientation of strongest coherent contribution. Example scattering distributions for different target positions and background positions are given in Fig. 3, with the obtained orientation at the peak of the coherent contribution and its -3 dB width indicated by blue circular marks.

2.3.3 Length Estimation

The length of a scatterer is most accurately estimated through its scattering response by first rotating the focused image wavenumber domain spectrum to align with the look angle to the broadside orientation θ. The rotated data can be averaged along the direction expressed by θ, giving the wavenumber domain response along the orientation of the scatterer. From this we can estimate the scatterer length in accordance with equation (3). However, for now we approximate the result by investigating the coherent scattering contribution as function of orientation as derived earlier for the orientation estimate and illustrated in Fig. 3. We assume that the angular response corresponds to that of the center frequency and use (4) to estimate the scatterer length.

$$\boxed{F(K_x, K_y)|_{(x_i,y_i)} \rightarrow F(\theta_o, \theta_{n_o})|_{(x_i,y_i)} \rightarrow f(\theta_{n_o})|_{(x_i,y_i)} \approx f(\theta)|_{(x_i,y_i)}}$$

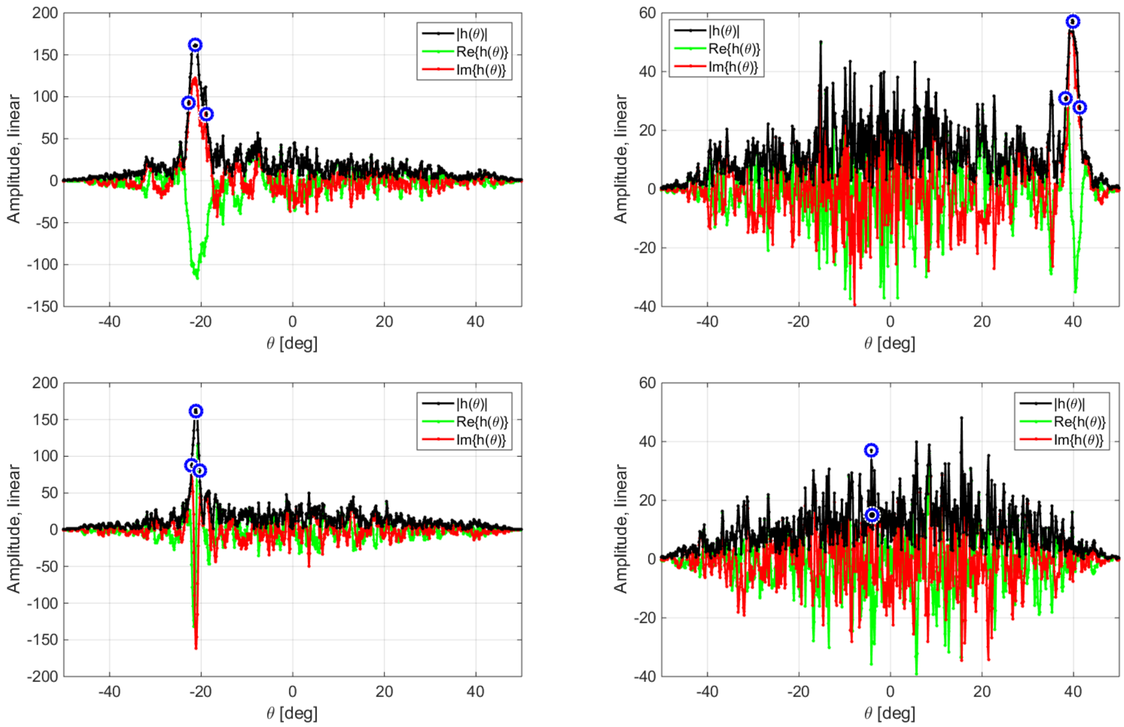

Fig. 3: $h(\theta)|_{(x,y)}$ *for focusing on 4 different points in the scene, together with the related estimations of orientation and beamwidth, indicated by blue circles. Top left: point at center of strong scattering line on "box". Top right; point on "frame". Bottom left: in "sidelobe" outside strong scattering line on "box". Bottom right: random pixel on the background.*

3. RESULTS AND DISCUSSION

In Fig. 4 we present the estimated orientation and effective scatterer length for the sample scene, and also include the LF SAS image for reference. Both orientation and effective length is expressed through color coding. The orientation is represented in a linear scale over the covered look angles, but note that the effective length is represented in a logarithmic scale. The minimum effective length corresponds to using the full 3dB bandwidth supported by the system, while the maximum effective length corresponds to a mainlobe width of two samples, c.f. equation (3).

We observe that the estimates are quite consistent for the strong scatterers that can be observed in the SAS image. The estimated orientations of -21 degrees and 40 degrees for the two objects are correct. The effective length of the strong scattering lines to the left are estimated to between 0.9 and 1.4 m correspond roughly to the observed length of 0.8 m for the lines. The effective length for the object on the right is estimated to between 1.1 and 1.4 m, which is a bit shorter than the actual length of 1.7 m. We have not yet investigated on the origin of this discrepancy.

For positions with background only, the vast majority of the estimates give random orientations and rather long scattering lengths. This would correspond to choosing a narrow random peak of coherent signal contribution (as illustrated in the lower right panel of Fig. 3), and is expected. For positions on the background that are along a linear extension of a strong scatterer, the estimates of these scatterers appear to extend onto the background. More advanced estimation of orientation and effective length might avoid this artefact, and if not, a mask might be provided to present the valid measurements.

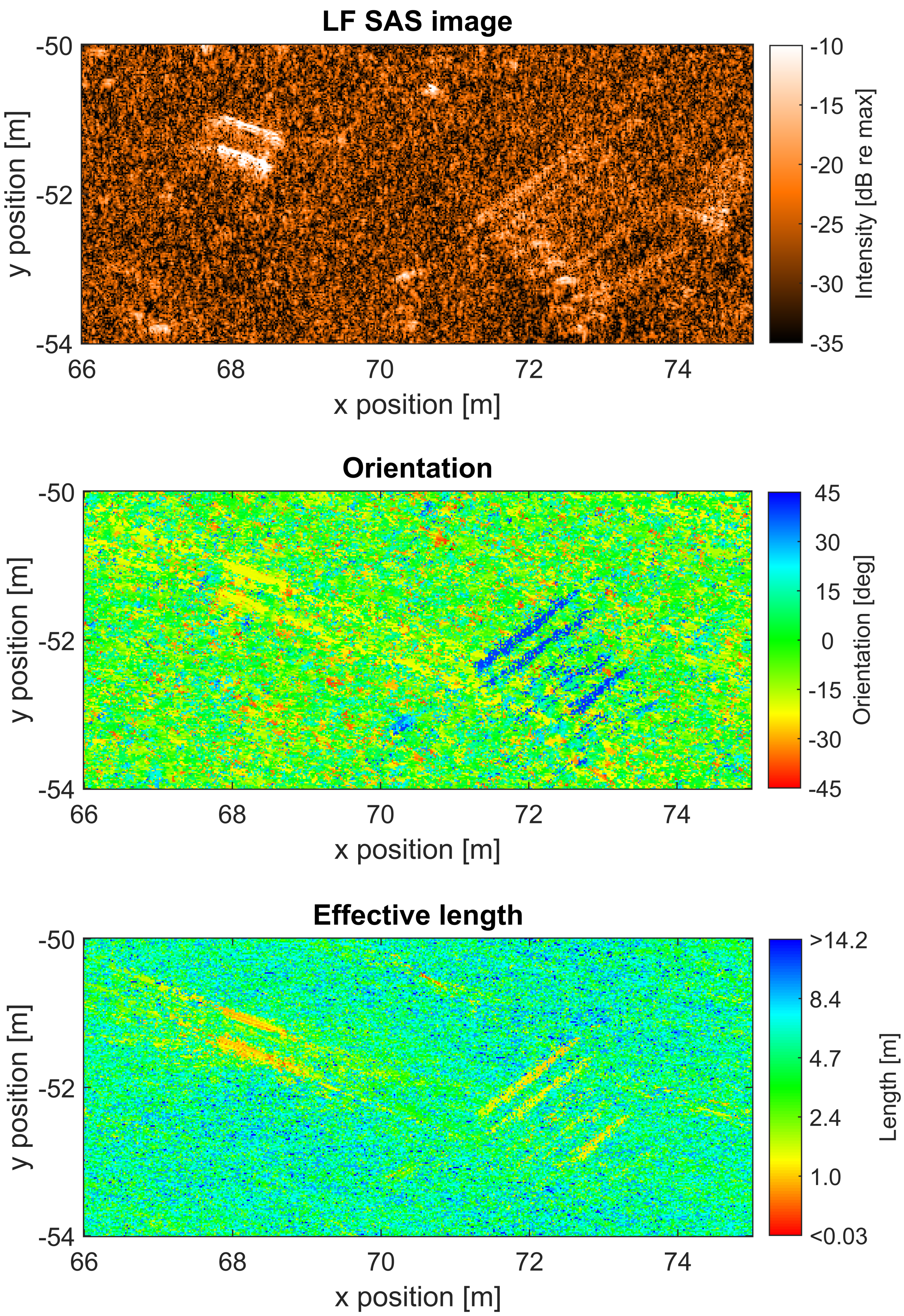

Fig. 4: The LF SAS image (top), together with the estimated orientation (center) and the estimated effective length (bottom).

4. CONCLUSION

Widebeam SAS gathers information on the aspect-dependency of the acoustic scattering. We have successfully demonstrated the estimation of orientation and effective length of facets, based on this aspect-dependent scattering represented in widebeam SAS images. In addition to providing orientation on facet orientation and length, the features can also support estimation of roughness and also be used for target segmentation.

Follow-up studies could investigate the effect of these new features on target detection and classification. Further studies could also investigate which related features can be extracted from a single pass when the specular reflection is not recorded, as with more narrowbeam (high frequency) SAS.

5. ACKNOWLEDGEMENTS

Thanks to Marc Geilhufe and Torstein Sœbø at FFI and Andreas Austeng at UiO for good feedback during the preparation of this paper.

REFERENCES

[1] R. Rau and J. H. McClellan. Analytic models and postprocessing techniques for UWB SAR. *IEEE Trans. Aerosp. and Electron. Syst.*, 36(4):1058–1074, 2000.

[2] M. R. Allen, S. A. Phillips, and D. J. Sofianos. Wide-angle SAR matched filter image formation for enhanced detection performance. In *SPIE 2093*, pages 381–387, 1994.

[3] R. D. Chaney, A. S. Willsky, and L. M. Novak. Coherent aspect-dependent SAR image formation. In *Proc. SPIE 2230*, pages 256–274, 1994.

[4] M. R. Allen, J. M. Jauregui, and L. E. Hoff. FOPEN-SAR detection by direct use of simple scattering physics. In *Proc. SPIE 2487*, pages 45–55, 1995.

[5] D. C. Brown, A. P. Lyons, and D. A. Cook. Spatial coherence theory and its application to synthetic aperture systems. In *SASSAR 2014, Institute of Acoustics Proceedings*, volume 36, pages 104–111, 2014.

[6] S. A. V. Synnes and R. E. Hansen. Ultra wideband SAS imaging. In *Underwater Acoustics Conference (UAC)*, 2013.

[7] S. A. V. Synnes, A. J. Hunter, R. E. Hansen, T. O. Sæbø, H. J. Callow, R. van Vossen, and A. Austeng. Wideband synthetic aperture sonar image formation and performance analysis. *To be submitted to IEEE Journal of Oceanic Engineering*, May 2015.

[8] J. Groen, R. E. Hansen, H. J. Callow, J. C. Sabel, and T. O. Sæbø. Shadow enhancement in synthetic aperture sonar using fixed focusing. 34(3):269–284, 2009.

[9] K. Baik, C. Dudley, and P. L. Marston. Acoustic quasi-holographic images of scattering by vertical cylinders from one-dimensional bistatic scans. *J. Acoust. Soc. Am.*, 130(6):3838–3851, 2011.